Unified Performance Analysis of Hybrid FSO/RF System With Diversity Combining

Long Huang, *Member, IEEE*, Siming Liu, Pan Dai, Mi Li, Gee-Kung Chang, *Fellow, IEEE*, Yuechun Shi, and Xiangfei Chen, *Senior Member, IEEE*

***Abstract*—Hybrid free space optical (FSO)/radio frequency (RF) systems have been proved to be reliable for high-data-rate wireless backhauls. In this article, we present a unified performance analysis of the hybrid FSO/RF transmission system which transmits identical data in both links and implements two popular diversity combining schemes, namely, selection combining (SC) and maximal ratio combining (MRC), in the receiver. Specially, for the FSO link, the Gamma-Gamma turbulence with pointing errors under heterodyne detection (HD) and intensity modulation/direction detection (IM/DD) is considered in our analysis while the general κ-μ shadowed fading which unifies popular RF fading models is employed for the analysis of the RF link. As a result, unified closed-form expressions of outage probabilities and average bit error rates for different modulation schemes are derived. A preliminary extension of the RF link to multi-input–multi-output (MIMO) transmission is also analyzed. Analytical and Monte Carlo simulation results are provided to characterize the performance of the hybrid FSO/RF link which is compared to the single FSO link and the single RF link. The agreement between the analytical and simulation results confirms the unification of various FSO channels and RF fading scenarios into a single closed-form expression.**

***Index Terms*—All-optical hybrid FSO/RF network, free space optics.**

I. Introduction

IN RECENT years, free space optical (FSO) communications have gained significant importance owing to the unique features: large bandwidth, ease of deployment, license free spectrum, lower power, less mass, small size, and improved channel security [1]. Despite these desirable advantages, FSO links are greatly affected by fading due to atmospheric turbulence and pointing errors [2], [3]. Turbulence-induced fading, known as scintillation, causes irradiance fluctuations in the received optical signal as a result of variations in the atmospheric refractive index [2]. Furthermore, dynamic wind loads and weak earthquakes cause vibrations of the optical beam, leading to random irradiance fluctuations in the received optical signal [3]. By employing multiple FSO links, the performance of FSO communication systems can be improved [4], [5]. However, all the FSO links still suffer from fog weather. A possible solution to improve the FSO link's reliability is to integrate it with a radio frequency (RF) link since the RF link exhibits complementary characteristics to weather conditions and supports data rates similar to those of FSO. Specifically, the FSO link degrades significantly due to fog but is not sensitive to rain while the RF link is very sensitive to rain but is quite indifferent to fog [6]. As a result, FSO and RF transmission systems are good candidates for joint deployment to provide reliable high data rate communications.

For the hybrid FSO/RF architecture, several studies have been reported on the system design. In [7]–[9], the data are jointly coded and divided into two streams which are transmitted by the FSO link and the RF link, respectively. The soft-switching between the two links has a significant improvement in the total link capacity. However, it is not suitable to implement the soft-switching in the fiber-wireless integrated mobile backhaul (MBH) architecture proposed in [10]. In the fiber-wireless integrated MBH architecture, the hybrid FSO/RF link provides a reliable link between the core network and base stations (BSs) where the RF signal is generated by photonic methods, leading to a scalable and cost-effective network setup. Therefore, if the soft-switching is employed in the fiber-wireless integrated MBH, the unencoded data carried by the optical carrier should be delivered from the core network to BSs. In the BS, the optical signal is converted to an electrical signal, and then a joint coding scheme is implemented, leading to two electrical coded streams. One coded stream is up-converted to the RF band by an RF front-end for the RF link while the other stream is converted back to an optical signal by an optical front-end for the FSO link. In the network architecture proposed in [10], the optical data stream is delivered to the BS from the core network and directly emitted for the FSO link, and the optical data stream can be

Manuscript received April 25, 2020; revised July 24, 2020 and August 16, 2020; accepted August 17, 2020. Date of publication August 20, 2020; date of current version December 15, 2020. This work was supported in part by the Chinese National Key Basic Research Special Fund under Grants 2017YFA0206401, 2018YFB2201801, and 2018YFA0704402, in part by National Natural Science Foundation of China under Grant 61975075, and in part by Science and Technology Project of Jiangsu province under Grant BE2019101. *(Corresponding author: Yuechun Shi.)*

Long Huang, Pan Dai, Mi Li, and Xiangfei Chen are with the Key Laboratory of Intelligent Optical Sensing and Manipulation of the Ministry of Education, and National Laboratory of Solid State Microstructures, College of Engineering and Applied Sciences, Institute of Optical Communication Engineering, Nanjing University, Nanjing 210093, China, and also with the Nanjing University (Suzhou) High-Tech Institute, Suzhou 215123, China (e-mail: draghuang@gmail.com; pdaiusc@gmail.com; limi@nju.edu.cn; chenxf@nju.edu.cn).

Siming Liu is with the Beijing University of Posts and Telecommunications, Beijing 100876, China (e-mail: siming.liu@ece.gatech.edu).

Gee-Kung Chang is with the School of Electrical and Computer Engineering, Georgia Institute of Technology, Atlanta, GA 30308 USA (e-mail: gkchang@ece.gatech.edu).

Yuechun Shi is with the College of Engineering and Applied Sciences, Nanjing University, Nanjing 210093, China (e-mail: shiyc@nju.edu.cn).

Color versions of one or more of the figures in this article are available online at https://ieeexplore.ieee.org.

Digital Object Identifier 10.1109/JLT.2020.3018125

up-converted to the RF signal at the same time by the photonic method, resulting in a simplified front-end design [11]–[14]. Based on this consideration, the scenario of transmitting identical data in both links is more suitable in the fiber-wireless integrated MBH. Previously, hard-switching between FSO and RF links which transmit the same data is proposed in [15]. In this scheme, the FSO link is used as the primary transmission channel as long as its signal-to-noise (SNR) is above a certain threshold value. When the SNR of the FSO link falls below the threshold, the receiver sends a feedback signal to activate the RF link for data transmission. To avoid the feedback transmission stage, diversity combining of the FSO link and the RF link can be implemented in the receiver. Two popular diversity combining schemes, namely selection combining (SC) and maximal ratio combining (MRC), are analyzed for the hybrid FSO/RF link with phase shift keying (PSK) modulation [16]. An outage analysis of the hybrid FSO/RF link is presented with MRC in [17]. The SC is also evaluated in the hybrid FSO/RF system [18], [19]. In terms of the FSO channel, pointing errors and two detection types, namely heterodyne detection (HD) or intensity modulation/direct detection (IM/DD), are not considered in [15]–[19]. As to the RF channel, the Rician fading is considered in [15], [16], and the Rayleigh fading is considered in [18], [19]. The MRC receiver used to combine the hybrid FSO/RF link is experimentally demonstrated in [10]. Although the atmospheric turbulence fading is emulated for the FSO link in [10], the pointing error, the detection type, and the RF fading are not considered in the experiment.

In this paper, we present a detailed outage and error rate analysis of the hybrid FSO/RF system where SC or MRC is used to combine the FSO and RF sub-links. The Gamma-Gamma turbulence-induced fading of the FSO link with pointing errors under HD and IM/DD is considered in our study. For the RF link, the operating frequency of the RF signal generated by beating two lasers can range from millimeter-wave to terahertz band [11]–[14]. As a result, a very general RF fading model which unifies many popular fading models including one-side Gaussian, Rayleigh, Nakagami-*m*, Rician, κ-μ, and Rician shadowed fading is used to analyze the hybrid FSO/RF link [20], [21]. To the best of our knowledge, this is the most general hybrid FSO/RF channel considered in the literature which can include as many scenarios as possible [15]–[19]. Furthermore, the multi-input multi-output (MIMO) transmission is a very mature technique to increase the channel capacity of RF links. On the contrary, the FSO has redundancy capacity compared to the RF link, and the MIMO setup of FSO links has not been widely employed leading to an expensive and unnecessary deployment. So, a hybrid MIMO RF link and single-input single-out (SISO) FSO link scenario is also considered in this paper. Novel closed-form results for the outage probability (OP) and average bit error rates (BERs) for different modulation schemes are derived in terms of the Fox's H function. The derived formulas are verified by Monte-Carlo simulations, and the most of hybrid FSO/RF scenarios can be quickly evaluated by the closed-form formulas.

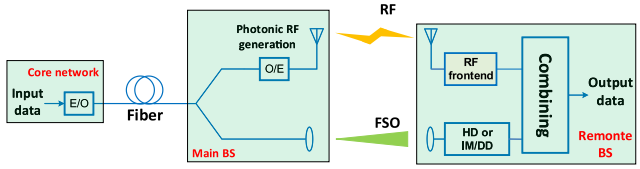

Fig. 1. Schematic diagram of the hybrid FSO/RF link incorporated in the fiber-wireless integrated MBH. LD: laser diode, E/O: electrical-to-optical conversion, O/E: optical-to-electrical conversion.

II. Principle

The schematic diagram of the hybrid FSO/RF system integrated in the fiber-wireless MBH proposed in [10] is shown in Fig. 1. The input data are delivered by the optical fiber from the service gateway and mobility management entity (S-GW/MME) of the core network to the main BS where the optical signal can be directly emitted by a telescope while a RF signal can be generated by the photonic method [11]–[14] which is widely used in high speed fiber-wireless systems. As a result, a hybrid FSO/RF link is established between the main BS and the remote BS to achieve reliable MBH.

A. FSO Subsystem

Firstly, the FSO sub-system of the hybrid FSO/RF link as shown in Fig. 1 is investigated specifically. For the transmitter of the FSO link, the modulated light is emitted by a telescope. In the receiver, the FSO link can be categorized into two classes based on the detection type: intensity modulation direct detection (IM/DD) and heterodyne detection (HD). In the HD system, the light is received by a telescope and then combined with a local oscillator beam. The HD system allow the amplitude and phase modulation of the optical field, leading to a considerable increase of the spectral efficiency compared to IM/DD at the expense of complexity. Typical modulation schemes used in HD consist of multilevel phase shift keying (M-PSK) or quadrature amplitude modulation (QAM). In IM/DD systems, the intensity of the transmitted light is employed to convey information. At the receiver side, the photo-detector directly detects changes in the received light intensity to recover the transmitted information. Typical modulation schemes used in the IM/DD system is OOK which can also be used in the HD system.

It is assumed that FSO receiver irradiance *I* can be expressed as $I = I_l I_a I_p$, where I_l is the path loss, I_a the atmospheric turbulence and I_p the pointing error [3]. Therefore, the probability density function (PDF) of the receiver irradiance *I* can be given by [3, Eq. (1)]

$$f_I(I) = \frac{\xi^2}{I\Gamma(\alpha)\Gamma(\beta)} G_{1,3}^{3,0}\left[\alpha\beta\frac{I}{A_0}\,\middle|\,\begin{matrix}\xi^2+1\\ \xi^2,\alpha,\beta\end{matrix}\right] \tag{1}$$

where ξ is the ratio between the equivalent beam radius and the pointing error displacement standard deviation at the receiver, A_0 is a constant term that represents the pointing loss, α and β are the fading/scintillation parameters related to the atmospheric turbulence conditions with lower values of α and β indicating

strong atmospheric turbulence conditions, and $G[.]$ is the Meijer's G function as defined in [22, Eq. (9.301)]. The parameters of α and β can be given by

$$\alpha = \left\{ \exp\left[\frac{0.49\sigma_l^2}{\left(1+0.18d^2+0.56\sigma_l^{12/5}\right)^{7/6}} \right] - 1 \right\}^{-1}$$

$$\beta = \left\{ \exp\left[\frac{0.51\sigma_l^2\left(1+0.69\sigma_l^{12/5}\right)^{-5/6}}{\left(1+0.9d^2+0.62\sigma_l^{12/5}\right)^{5/6}} \right] - 1 \right\}^{-1}$$

where $\sigma_l^2 = 0.5C_n^2 k^{7/6} L^{11/6}$ is the log irradiance variance, $d = (kD^2/4L)^{1/2}$ ($k = 2\pi/\lambda$, λ denotes the wavelength, L is the FSO propagation path length, D is the diameter of the receiver collecting lens aperture), and $C_n{}^2$ represents the refractive index structure.

Both of HD and IM/DD are considered in our paper. Then, a unified expression of the SNR per symbol in the receiver can be given by $\gamma_r = (\eta_e I)^r/N_0$, where η_e is the optical-to-electrical conversion ratio, r is the parameter which denotes the type of detection being used (i.e. $r = 1$ is associated with HD and $r = 2$ associated with IM/DD), and N_0 is the additive white Gaussian noise. Therefore, a unified expression of PDF of γ_r including both HD and IM/DD can be derived from Eq. (1) and is given by [23, Eq. (2)],

$$f_\gamma^{FSO}(\gamma_r) = \frac{\xi^2}{r\Gamma(\alpha)\Gamma(\beta)\gamma} G_{1,3}^{3,0}\left[\alpha\beta h\left(\frac{\gamma_r}{\mu_r}\right)^{\frac{1}{r}} \middle| \begin{matrix} \xi^2+1 \\ \xi^2, \alpha, \beta \end{matrix} \right] \tag{2}$$

Where $h = \xi^2/(\xi^2+1)$, and $\mu_r = (\mathrm{E}[\eta_e I])^r/N_0$ refers to the average electrical SNR. In particular, for $r = 1$,

$$\mu_1 = \mu_{HD} = A_0\eta_e\xi^2/[(1+\xi^2)N_0] = \bar{\gamma}_1 \tag{3}$$

and for $r = 2$,

$$\mu_2 = \mu_{IM/DD} = \frac{A_0^2\eta_e^2\xi^4}{(1+\xi^2)^2 N_0} = \frac{\alpha\beta\xi^2(\xi^2+2)}{(\alpha+1)(\beta+1)(\xi^2+1)}\bar{\gamma}_2. \tag{4}$$

Using [22, Eq. (3.381.4)], the moment generating function (MGF) of γ_r can be given by

$$\begin{aligned} M_\gamma^{FSO}(s) &= \mathrm{E}\left[e^{s\gamma_r}\right] \\ &= \int_0^\infty f_\gamma^{FSO}(\gamma_r) e^{s\gamma_r} d\gamma_r \\ &= \frac{\xi^2}{r\Gamma(\alpha)\Gamma(\beta)} H_{2,3}^{3,1} \\ &\quad \left[\alpha\beta h\left(\frac{-1}{\mu_r s}\right)^{\frac{1}{r}} \middle| \begin{matrix} (1,1/r),(\xi^2+1,1) \\ (\xi^2,1),(\alpha,1),(\beta,1) \end{matrix} \right] \end{aligned} \tag{5}$$

where $H[.]$ is the Fox's H function defined in [24], and E[.] is the mathematical expectation. The cumulative density function (CDF) can be given by [23, Eq. (7)],

$$F_\gamma^{FSO}(\gamma_r) = 1 - \frac{\xi^2}{\Gamma(\alpha)\Gamma(\beta)} G_{2,4}^{4,0}\left[\alpha\beta h\left(\frac{\gamma_r}{\mu_r}\right)^{\frac{1}{r}} \middle| \begin{matrix} 1, \xi^2+1 \\ 0, \xi^2, \alpha, \beta \end{matrix} \right]. \tag{6}$$

Hence, the OP which is defined as the probability when the SNR falls below a predetermined protection threshold γ_{th} can be directly obtained by replacing γ_r with γ_{th} in Eq. (6), that is, $P_{out}^{FSO} = F_\gamma^{FSO}(\gamma_{th})$. Using the CDF expression, a unified expression of the average BER can be given by [23, Eq. (22)]

$$P_e = \frac{\delta}{2\Gamma(p)} \sum_{k=1}^{n} q_k^p \int_0^\infty \gamma^{p-1} e^{-q_k\gamma} F_\gamma(\gamma) d\gamma \tag{7}$$

where n, δ, p, and q_k depend on detection types and modulation being assumed according to Table I. It is worth noting that this expression is general enough to be used for different modulation schemes and can also be applicable to RF channels. As a result, the average BER of the FSO link can be given by

$$\begin{aligned} P_e^{FSO} = \frac{n\delta}{2} - \frac{\delta\xi^2}{2\Gamma(p)\Gamma(\alpha)\Gamma(\beta)} \sum_{k=1}^{n} H_{3,4}^{4,1} \\ \left[\alpha\beta h(q_k\mu_r)^{-\frac{1}{r}} \middle| \begin{matrix} (1-p,1/r)(1,1)(\xi^2+1,1) \\ (0,1)(\xi^2,1)(\alpha,1)(\beta,1) \end{matrix} \right]. \end{aligned} \tag{8}$$

The derivation of Eq. (8) is given in Appendix A.

B. RF Subsystem

The fiber-wireless integration system can generate RF signal by photonic methods which promotes the seamless integration of wireless and fiber-optics network. In the RF link, the generated RF signal is emitted by an antenna and received by a conventional RF frontend. The propagation of RF signals suffers from multipath fading. The κ-μ shadowed fading which includes several RF channel models such as Nakagami-m, Rayleigh, Rician, κ-μ, and shadowed Rician fading distributions offers better and much more flexible representations of practical fading than Rayleigh and Rician fading considered in previous hybrid FSO/RF systems [15]–[19]. The PDF of instantaneous SNR γ of the κ-μ shadowed fading with non-negative real shape parameters κ, μ and m is expressed as [20, Eq. (4)]

$$\begin{aligned} f_\gamma^{RF}(\gamma) = \frac{\mu^\mu m^m (1+\kappa)^\mu}{\Gamma(\mu)\bar{\gamma}(\mu\kappa+m)^m} \left(\frac{\gamma}{\bar{\gamma}}\right)^{\mu-1} \\ \times e^{-\frac{\mu(1+\kappa)\gamma}{\bar{\gamma}}} {}_1F_1\left(m, \mu; \frac{\mu^2\kappa(1+\kappa)}{\mu\kappa+m}\frac{\gamma}{\bar{\gamma}}\right) \end{aligned} \tag{9}$$

where ${}_1F_1(.)$ is the confluent hypergeometric function [20]. However, the confluent hypergeometric function leads to a very complicated form if not unresolvable. In [21], the κ-μ shadowed distribution is expressed as a mixture of squared Nakagami-$\hat{m}$ distributions when μ and m take integer values. Thus, the PDF can be expressed in closed-form in terms of a finite number of elementary functions (powers and exponentials). It is demonstrated in [21] such restriction has little effect in practice when fitting field measurements to the κ-μ shadowed distribution,

TABLE I
PARAMETERS FOR DIFFERENT MODULATIONS

Modulation Scheme		p	q_k	n	Detection Type
OOK	1	1/2	1/2	1	FSO(IM/DD), RF
M-PSK	$\frac{2}{\max(\log_2 M,2)}$	1/2	$\sin^2\left(\frac{(2k-1)\pi}{M}\right)$	$\max\left(\frac{M}{4},1\right)$	FSO(HD), RF
M-QAM	$\frac{4}{\log_2 M}\left(1-\frac{1}{\sqrt{M}}\right)$	1/2	$\frac{3(2k-1)^2}{2(M-1)}$	$\frac{\sqrt{M}}{2}$	FSO(HD), RF
CBFSK	1	1/2	1/2	1	FSO(HD), RF
NBFSK	1	1	1/2	1	FSO(IM/DD), RF
DBPSK	1	1	1	1	FSO(HD), RF

while being extremely convenient for computation. The PDF with integer μ and m can be expressed as [21, Eq. (12)]

$$f_\gamma^{RF}(\gamma)=\sum_{i=0}^{M} C_i \frac{\gamma^{m_i-1}}{(m_i-1)!}\frac{1}{\Omega_i^{m_i}} e^{-\frac{\gamma}{\Omega_i}} \tag{10}$$

where parameters m_i, M and Ω_i are expressed in [21, Table I] in terms of the parameters of κ-μ shadowed distribution, namely, κ, μ and m. Using [22, Eq. (9.301)], the MGF of SNR can be written as

$$\begin{aligned} M_\gamma^{RF}(s) &= \int_0^\infty f_\gamma^{RF}(\gamma)e^{s\gamma}d\gamma \\ &= \sum_{i=0}^{M}\frac{C_i}{(m_i-1)!}\frac{\Gamma(m_i)}{(1-\Omega_i s)^{m_i}} \\ &= \sum_{i=0}^{M}\frac{C_i}{(m_i-1)!}G_{1,1}^{1,1}\left(-s\Omega_i\middle|\begin{matrix}1-m_i\\0\end{matrix}\right). \end{aligned} \tag{11}$$

The CDF of κ-μ shadowed distribution can be expressed as [21, Eq. (13)]

$$F_\gamma^{RF}(\gamma)=1-\sum_{i=0}^{M} C_i e^{-\frac{\gamma}{\Omega_i}}\sum_{r=0}^{m_i-1}\frac{1}{r!}\left(\frac{\gamma}{\Omega_i}\right)^r. \tag{12}$$

Therefore, the OP of the RF link can be given by $P_{out}^{RF}=F_\gamma^{RF}(\gamma_{th})$. By using Eq. (12) and [22, Eq. (3.381.4)], the average BER of the RF link can be written as

$$\begin{aligned} P_e^{RF} &= \frac{\delta}{2\Gamma(p)}\sum_{k=1}^{n} q_k^p \int_0^\infty \gamma^{p-1}e^{-q_k\gamma}F_\gamma^{RF}(\gamma)d\gamma \\ &= \frac{\delta n}{2}-\frac{\delta}{2\Gamma(p)}\sum_{k=1}^{n}\sum_{i=0}^{M}\sum_{r=0}^{m_i-1}\frac{C_i\Gamma(p+r)}{r!}\frac{1}{\Omega_i^r(q_k+1/\Omega_i)^{p+r}} \end{aligned} \tag{13}$$

where n, δ, p, and q_k for different modulation schemes are given in Table I.

C. FSO/RF Link With Diversity Combining

In the hybrid FSO/RF link, diversity combining is implemented in the receiver to combine the FSO sub-link and the RF sub-link. Two popular diversity combining schemes, SC and MRC, are employed for the analysis of the hybrid FSO/RF link.

For the SC receiver, the received signal of each sub-system is combined such that the SNR is the maximum of the two sub-links [16], i.e.,

$$\gamma^{SC}=\max(\gamma^{FSO},\gamma^{RF}). \tag{14}$$

Then the CDF of the SC can be given by

$$\begin{aligned} &F_\gamma^{SC}(\gamma) \\ &= F_\gamma^{FSO}(\gamma)F_\gamma^{RF}(\gamma) \\ &= 1-\frac{\xi^2}{\Gamma(\alpha)\Gamma(\beta)}G_{2,4}^{4,0}\left[\alpha\beta h\left(\frac{\gamma_r}{\mu_r}\right)^{\frac{1}{r}}\middle|\begin{matrix}1,\xi^2+1\\0,\xi^2,\alpha,\beta\end{matrix}\right] \\ &\quad-\sum_{i=0}^{M}\sum_{r=0}^{m_i-1}\frac{C_i}{r!}e^{-\frac{\gamma}{\Omega_i}}\left(\frac{\gamma}{\Omega_i}\right)^r \\ &\quad+\frac{\xi^2}{\Gamma(\alpha)\Gamma(\beta)}\sum_{i=0}^{M}\sum_{r=0}^{m_i-1}\frac{C_i}{r!}e^{-\frac{\gamma}{\Omega_i}}\left(\frac{\gamma}{\Omega_i}\right)^r \\ &\quad\times G_{2,4}^{4,0}\left[\alpha\beta h\left(\frac{\gamma}{\mu_r}\right)^{\frac{1}{r}}\middle|\begin{matrix}1,\xi^2+1\\0,\xi^2,\alpha,\beta\end{matrix}\right] \\ &= F_\gamma^{FSO}(\gamma)-\sum_{i=0}^{M}\sum_{r=0}^{m_i-1}\frac{C_i}{r!}e^{-\frac{\gamma}{\Omega_i}}\left(\frac{\gamma}{\Omega_i}\right)^r \\ &\quad+\frac{\xi^2}{\Gamma(\alpha)\Gamma(\beta)}\sum_{i=0}^{M}\sum_{r=0}^{m_i-1}\frac{C_i}{r!}e^{-\frac{\gamma}{\Omega_i}}\left(\frac{\gamma}{\Omega_i}\right)^r \\ &\quad\times G_{2,4}^{4,0}\left[\alpha\beta h\left(\frac{\gamma}{\mu_r}\right)^{\frac{1}{r}}\middle|\begin{matrix}1,\xi^2+1\\0,\xi^2,\alpha,\beta\end{matrix}\right]. \end{aligned} \tag{15}$$

The OP of the SC receiver can be obtained by $P_{out}^{MRC}=F_\gamma^{MRC}(\gamma_{th})$. The average BER for OOK, M-PSK and M-QAM with the SC receiver can be given by

$$P_e^{SC}=\frac{n\delta}{2}-\frac{\delta\xi^2}{2\Gamma(p)\Gamma(\alpha)\Gamma(\beta)}\sum_{k=1}^{n}H_{3,4}^{4,1}$$

$$\left[\alpha\beta h(q_k\mu_r)^{-\frac{1}{r}}\middle|\begin{matrix}(1-p,1/r)(1,1)(\xi^2+1,1)\\(0,1)(\xi^2+1)(\alpha+1)(\beta+1)\end{matrix}\right]$$

$$- \frac{\delta}{2\Gamma(p)} \sum_{k=1}^{n} \sum_{i=0}^{M} \sum_{r=0}^{m_i-1} \frac{C_i \Gamma(p+r)}{r!} \frac{1}{\Omega_i^r (q_k + \Omega_i^{-1})^{p+r}}$$

$$+ \frac{\delta}{2\Gamma(p)} \frac{\xi^2}{\Gamma(\alpha)\Gamma(\beta)} \sum_{k=1}^{n} \sum_{i=0}^{M} \sum_{r=0}^{m_i-1} \frac{q_k^p C_i}{r! \Omega_i^r} \left(q_k + \Omega_i^{-1}\right)^{-p-r}$$

$$\cdot H_{3,4}^{4,1}\left[\alpha\beta h((q_k+\Omega_i^{-1})\mu_r)^{-1/r} \middle| \begin{matrix}(1-p-r,1/r)(1,1)(\xi^2+1,1)\\ (0,1)(\xi^2,1)(\alpha,1)(\beta,1)\end{matrix}\right]. \tag{16}$$

The derivation of Eq. (16) is given in Appendix B.

For the MRC receiver of the hybrid FSO/RF link, the combined signal is $S_c = w_1 S_{FSO} + w_2 S_{RF}$, where S_{FSO} and S_{RF} are the FSO and RF signals, respectively. The combining weights w_1 and w_2 are given by$w_1 = c(h_{FSO})^*/\sigma_1^2$ and$w_2 = c(h_{RF})^*/\sigma_2^2$, where h_{FSO} is the FSO channel response, σ_1 is the standard deviation of noise of the FSO link, h_{RF} is the RF channel response, σ_2 is the standard deviation of noise of the RF link, and c is any complex number.

At the output of the MRC, the combined SNR is the sum of the SNR of each sub-link [10]–[16], i.e.,

$$\gamma^{MRC} = \gamma^{FSO} + \gamma^{RF}. \tag{17}$$

Therefore, the MGF of the SNR of the MRC receiver can be given by

$$\begin{aligned} M_\gamma^{MRC}(s) &= \mathrm{E}[e^{s\gamma^{MRC}}] = \mathrm{E}[e^{s\gamma^{FSO}}]\mathrm{E}[e^{s\gamma^{RF}}] \\ &= M_\gamma^{FSO}(s) M_\gamma^{RF}(s). \end{aligned} \tag{18}$$

The CDF can be found from the inverse Laplace transform of $M_\gamma^{MRC}(-s)/s$, which can be expressed as

$$F_\gamma^{MRC}(\gamma) = \mathcal{L}^{-1}\left(M_\gamma^{MRC}(-s)/s\right)$$

$$= \frac{\xi^2}{r\Gamma(\alpha)\Gamma(\beta)} \sum_{i=0}^{M} \frac{C_i}{(m_i-1)!} H_{1,1:1,1:2,3}^{0,1:1,1:3,1}$$

$$\times \left[\begin{matrix} \frac{\gamma}{\Omega_i} \\ \alpha\beta h(\gamma/\mu_r)^{1/r} \end{matrix} \middle| \begin{matrix} -:(1,1):(1,\frac{1}{r})(\xi^2+1,1) \\ (0,1,\frac{1}{r}):(m_i,1):(\xi^2,1)(\alpha,1)(\beta,1) \end{matrix} \right]. \tag{19}$$

The derivation of Eq. (19) is given in Appendix C.

The OP of the MRC receiver can be obtained by $P_{out}^{MRC} = F_\gamma^{MRC}(\gamma_{th})$. Finally, the average BER of OOK, M-PSK and M-QAM for the MRC receiver can be given by

$$P_e^{MRC}$$

$$= \frac{\delta\xi^2}{2r\Gamma(\alpha)\Gamma(\beta)\Gamma(p)}$$

$$\cdot \sum_{k=1}^{n} \sum_{i=0}^{M} \frac{C_i}{(m_i-1)!} H_{1,1:1,1:2,3}^{0,1:1,1:3,1}$$

$$\left[\begin{matrix} \frac{1}{q_k\Omega_i} \\ \alpha\beta h\left(\frac{1}{\mu_r q_k}\right)^{\frac{1}{r}} \end{matrix} \middle| \begin{matrix} (p,1,\frac{1}{r}):(1,1):(1,\frac{1}{r})(\xi^2+1,1) \\ (0,1,\frac{1}{r}):(m_i,1):(\xi^2,1)(\alpha,1)(\beta,1) \end{matrix} \right]. \tag{20}$$

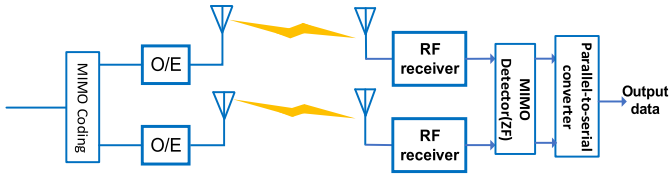

Fig. 2. Diagram of MIMO RF link.

The derivation of Eq. (20) is given in Appendix D.

To the best of our knowledge, the derived closed-form formulas of the hybrid FSO/RF link are the most general in literature, which can be adapted to different FSO and RF channel conditions. As a result, the detection types, i.e. HD and IM/DD, the pointing errors and turbulence fading can be evaluated qualitatively.

D. Hybrid FSO and MIMO RF Link With Diversity Combining

MIMO technique has been employed in fiber-wireless integration system to increase the capacity of the RF link [25], [26]. On the other hand, the FSO link has redundant capacity compared to the RF link. As a result, the hybrid MIMO RF link and SISO FSO link is a feasible and practical scenario. As shown in Fig. 2, the data stream in the MIMO RF link is demultiplexed into a number of data sub-streams which are sent by corresponding transmitter antennas. At the receiver, the signals are received by multiple receiver antennas and detected by a zero-forcing (ZF) detector. Finally, the detected signals are sent to parallel-to-serial converter and combined with FSO signals.

For the MIMO RF link, the received signal can be expressed as

$$\boldsymbol{y} = \boldsymbol{H}\boldsymbol{d} + \boldsymbol{n} \tag{21}$$

where $\boldsymbol{y} = [y_1 \ldots y_{rx}]^{\mathrm{T}}$ is the received signal vector, $\boldsymbol{H}$ is a rx $\times$ tx channel matrix containing elements $h_{i,j}$, $\boldsymbol{d} = [d_1 \ldots d_{tx}]^T$ is the transmitted symbol vector and $n = [n_1 \ldots n_{rx}]^T$ is the noise vector. The elements of $\boldsymbol{H}$ are assumed as circularly symmetric complex Gaussian (CSCG) random variables, and the elements of $\boldsymbol{n}$ are taken to be i.i.d Gaussian random variables with zero mean and variance σ'^2.

The MIMO zero forcing (ZF) detector is designed to completely eliminate the inter-stream interference (ISI) [25]–[27]. As a result, the estimated data vector, denoted by $\hat{\boldsymbol{d}}$ is given by

$$\hat{\boldsymbol{d}} = \boldsymbol{H}^+(\boldsymbol{H}\boldsymbol{d} + \boldsymbol{n}) = \boldsymbol{d} + \boldsymbol{H}^+\boldsymbol{n} = \boldsymbol{d} + \boldsymbol{e} \tag{22}$$

where $\boldsymbol{H}^+ = (\boldsymbol{H}^H\boldsymbol{H})^-\boldsymbol{H}^H$ is the pseudo-inverse of $\boldsymbol{H}$. The post-detection SNR with the ZF detector can be expressed as

$$\gamma_k = \frac{\mathrm{E}[|d_k|^2]}{\mathrm{E}[\boldsymbol{e}\boldsymbol{e}^H]_{kk}} = \frac{\mathrm{E}[|d_k|^2]}{\sigma^2[\boldsymbol{H}^H\boldsymbol{H}]_{kk}^{-1}} = \frac{\gamma_0}{[\boldsymbol{H}^H\boldsymbol{H}]_{kk}^{-1}}, k = 1, \ldots, tx \tag{23}$$

where $\gamma_0 = \mathrm{E}[|d_k{}^2|]/\sigma^2$ is the normalized received SNR per symbol at each receive antenna.

We assume the MIMO channel is i.i.d Rayleigh fading channel. Then the PDF of γ_k is given by [27]

$$f(\gamma_k) = \frac{\exp(-\gamma_k/\gamma_0)}{\gamma_0\Gamma(rx - tx + 1)} \left(\frac{\gamma_k}{\gamma_0}\right)^{rx-tx}. \tag{24}$$

Furthermore, the CDF of γ_k can be expressed as [27]

$$F(\gamma_k) = \frac{\gamma(rx - tx + 1, \gamma_k/\gamma_0)}{\Gamma(rx - tx + 1)}. \tag{25}$$

where $\gamma(a, z)$ denotes the incomplete Gamma function. Besides, the MGF of the MIMO RF link is given by

$$M_\gamma^{RF}(s) = \left(\frac{1}{1 - s\gamma_0}\right)^{rx-tx+1}. \tag{26}$$

The spatial-multiplexed data are also sent by a SISO FSO link, the received signal η can be expressed

$$\eta_k = h_{FSO} d_k + z \tag{27}$$

where h_{FSO} denotes the FSO channel, d_k denotes the data sent by the k-th antenna of the RF link, and z is the noise term with zero mean and σ'^2 variance. The SNR of SISO FSO link is $\gamma_{FSO} = |h_{FSO}|^2 \mathrm{E}[|d_k|^2]/\sigma'^2$.

For the SC scenario, the receiver chooses the maximal SNR of the RF link and the FSO link, and then the CDF of the combined signal can be given by

$$\begin{aligned} F^{SC}(\gamma) &= F^{FSO}(\gamma) F^{RF}(\gamma) \\ &= \frac{\gamma\left(rx - tx + 1, \frac{\gamma}{\gamma_0}\right)}{\Gamma(rx - tx + 1)} - \frac{\xi^2}{\Gamma(\alpha)\Gamma(\beta)\Gamma(rx - tx + 1)} \\ &\cdot G_{2,4}^{4,0}\left[\alpha\beta h\left(\frac{\gamma}{\mu_r}\right)^{\frac{1}{r}} \middle| \begin{matrix} 1, \xi^2 + 1 \\ 0, \xi^2, \alpha, \beta \end{matrix}\right] \gamma\left(rx - tx + 1, \frac{\gamma}{\gamma_0}\right) \end{aligned} \tag{28}$$

Therefore, the BER of the SC receiver is expressed as Eq. (29) shown at the bottom of this page.

For the MRC scenario, the two links are coherently combined such that the combined SNR is the sum of the two links. The combining weights are w_k for the k-th data stream, and v_k for the corresponding stream transmitted by the FSO link. The combined signal can be expressed as

$$S_k = w_k \hat{d}_k + v_k \eta_k = (w_k + v_k h_{FSO})\, d_k + w_k e_k + v_k z. \tag{30}$$

The combined SNR can be given by

$$\gamma_k^{MRC} = \frac{|w_k + v_k h_{FSO}|^2}{|w_k|^2 \sigma^2 [\boldsymbol{H}^H \boldsymbol{H}]_{kk}^{-1} + |v_k|^2 \sigma'^2} \mathrm{E}[|d_k|^2]. \tag{31}$$

Using Cauchy-Schwarz inequality, the combined SNR can be expressed as

$$\begin{aligned} &\gamma_k^{MRC} \\ &\le \left[|w_k|^2 \sigma^2 [\boldsymbol{H}^H \boldsymbol{H}]_{kk}^{-1} + |v_k|^2 \sigma'^2\right] \\ &\cdot \frac{\left(\frac{1}{\sigma^2 [\boldsymbol{H}^H \boldsymbol{H}]_{kk}^{-1}} + \frac{|h_{FSO}|^2}{\sigma'^2}\right) \mathrm{E}[|d_k|^2]}{|w_k|^2 \sigma^2 [\boldsymbol{H}^H \boldsymbol{H}]_{kk}^{-1} + |v_k|^2 \sigma'^2} \\ &= \left(\frac{1}{\sigma^2 [\boldsymbol{H}^H \boldsymbol{H}]_{kk}^{-1}} + \frac{|h_{FSO}|^2}{\sigma'^2}\right) \mathrm{E}[|d_k|^2] \\ &= \gamma_k + \gamma_{FSO} \end{aligned} \tag{32}$$

where equality holds iff

$$w_k = c \frac{1}{\sigma^2 [\boldsymbol{H}^H \boldsymbol{H}]_{kk}^{-1}}, v_k = c \frac{h_{FSO}^*}{\sigma'^2} \tag{33}$$

with c being any complex number.

For the MRC receiver which chooses the combined weights given in Eq. (33), the CDF of the hybrid link can be given by

$$\begin{aligned} &F_\gamma^{MRC}(\gamma) \\ &= \frac{1}{2\pi j} \int_{\sigma - j\infty}^{\sigma + j\infty} \frac{M_\gamma^{MRC}(-s)}{s} e^{s\gamma} ds \\ &= \frac{1}{2\pi j} \int_{\sigma - j\infty}^{\sigma + j\infty} \frac{M_\gamma^{FSO}(-s) M_\gamma^{RF}(-s)}{s} e^{s\gamma} ds \\ &= \frac{1}{2\pi j} \int_{\sigma - j\infty}^{\sigma + j\infty} \frac{\xi^2}{r\Gamma(\alpha)\Gamma(\beta)} H_{2,3}^{3,1} \\ &\left[\alpha\beta h (\mu_r s)^{-1/r} \middle|_{(\xi^2,1)(\alpha,1)(\beta,1)}^{(1,1/r)(\xi^2+1,1)}\right] \left(\frac{1}{1 + s\gamma_0}\right)^{rx-tx+1} e^{s\gamma} s^{-1} ds \\ &= \frac{\xi^2}{r\Gamma(\alpha)\Gamma(\beta)} \frac{(\gamma/\gamma_0)^{rx-tx+1}}{\Gamma(1 + rx - tx)} \cdot H_{0,1;2,3;1,1}^{0,0;3,1;1,1} \\ &\left[\begin{matrix} \alpha\beta h (\gamma/\mu_r)^{1/r} \\ \gamma/\gamma_0 \end{matrix} \middle| \begin{matrix} --:(1,1/r)(\xi^2+1,1):(tx-rx,1) \\ (-1-rx+tx;1/r,1):(\xi^2,1)(\alpha,1)(\beta,1):(0,1) \end{matrix}\right]. \end{aligned} \tag{34}$$

Using the CDF, the BER of the hybrid link can be expressed as Eq. (35) shown at the bottom of the next page.

III. Numerical Results

A. Hybrid FSO and SISO RF Link

In this sub-section, numerical results are provided to investigate the performance of the hybrid FSO/RF link compared to the single FSO link and the single RF link. The analytical plots are obtained by using the derived formulas in the previous section, and Monte Carlo simulation results are obtained through MATLAB to prove the correctness of the theoretical results.

For the FSO link, the Gamma-Gamma fading with the effects of atmosphere for weak, moderate, and strong turbulence is investigated. The values of all the parameters used in calculations

$$P_e = \frac{\delta}{2\Gamma(p)} \cdot \sum_{k=1}^{n} \left[\begin{matrix} \frac{G_{2,2}^{1,2}\left(\frac{1}{q\gamma_0} \middle| \begin{matrix} 1, 1-p \\ rx - tx + 1, 0 \end{matrix}\right)}{\Gamma(rx-tx+1)} - \frac{\xi^2}{\Gamma(\alpha)\Gamma(\beta)\Gamma(rx-tx+1)} \\ \cdot H_{1,0:2,4;1,2}^{0,1:4,0;1,1} \left[\begin{matrix} \alpha\beta h (1/(\mu_r q))^{\frac{1}{r}} \\ 1/(q\gamma_0) \end{matrix} \middle| \begin{matrix} (1-p, 1/\rho, 1):(1,1)(\xi^2+1,1);(1,1) \\ -:(0,1)(\xi^2,1)(\alpha,1)(\beta,1);(rx-tx+1,1)(0,1) \end{matrix}\right] \end{matrix} \right] \tag{29}$$

TABLE II
SIMULATION PARAMETERS WITH RESPECT TO WEAK, MODERATE AND STRONG TURBULENCE REGIMES

Wavelength		λ=1550 nm
Refractive index		$C_n^2 = 1.7\times10^{-14}$
Diameter of the receiver		$D \ll L$ and $d = 0$
Link length $L = 3$ km	σ_l^2=1.03	α=2.902 β=2.51 weak
Link length $L = 4$ km	σ_l^2=1.75	α=2.296 β=1.822 moderate
Link length $L = 6$ km	σ_l^2=3.67	α=2.064 β=1.342 strong

are illustrated in Table II [30]. Furthermore, the effect of the pointing error is characterized by the following parameters: $A_0 = [\mathrm{erf}(\nu)]^2$, $\nu = \sqrt{\pi/2}R/w_b$, $\xi^2 = {w_e}^2/(4{\sigma_s}^2)$, R is the radius of the Rx aperture, w_b is the received beam size, $w_e = [\sqrt{\pi}erf(v)w_b^2/(2ve^{-v^2})]^{1/2}$ is the equivalent beamwaist, ${\sigma_s}^2$ is the variance of the Gaussian distributions for both horizontal and vertical buildings' sway (i.e., point error displacement variance), and erf(·) denotes the error function. In the simulation, the pointing error is varied as $\xi = 10.45, 2.15, 1.45, 1.15, 0.95, 0.65, 0.45$ with $A_0 = 1$, where a smaller value of ξ means a larger pointing error. The fading parameters κ, μ and m are adjusted in the simulation to represent different channel conditions.

In the first simulation, the pointing error ξ is set to 1. The RF link is supposed to be subjected to Rician shadowed fading ($\kappa = 5$, $\mu = 1$, $m = 2$). The analytical OPs of the single FSO link and the hybrid FSO/RF link are calculated successively, and the simulated OPs are also plotted in the same figure. Figs. 3(a)–Figs. 3(c) illustrate the OP of the FSO link and the hybrid FSO/RF link versus the average SNR of the FSO link under weak, moderate and strong turbulence, respectively. In Fig. 3, the average SNR of the RF link is set to 10 dB.

As can be seen from Fig. 3(a), the HD is better than the IM/DD. When the average SNR of the single FSO link is 20 dB, the OP of the single FSO link under HD is 2.51×10^{-2} while that under IM/DD increases to 1.63×10^{-1}. The performance of the hybrid FSO/RF link can be improved along with the improvement of the FSO sub-link, so the OP of the hybrid FSO/RF link under HD is also better than that under IM/DD. For example, the OP of the hybrid FSO/RF link with the SC receiver under HD is 2.91×10^{-3} while that under IM/DD increases to 1.89×10^{-2}. Furthermore, the OP of the hybrid FSO/RF link with the MRC receiver under HD is 1.40×10^{-3} while that under IM/DD increases to 1.26×10^{-2}.

From Fig. 3(a), the hybrid FSO/RF link has better performance than the single FSO link. Moreover, the MRC receiver performs better than the SC receiver although its practical implement is more complex. For example, when the average SNR of the FSO link is 30 dB and the detection type is HD, the OP of the single FSO link is 2.53×10^{-3}. The OP of the hybrid FSO/RF link with the SC receiver is improved to 2.90×10^{-4} while that with the MRC receiver is further improved to 1.42×10^{-4}.

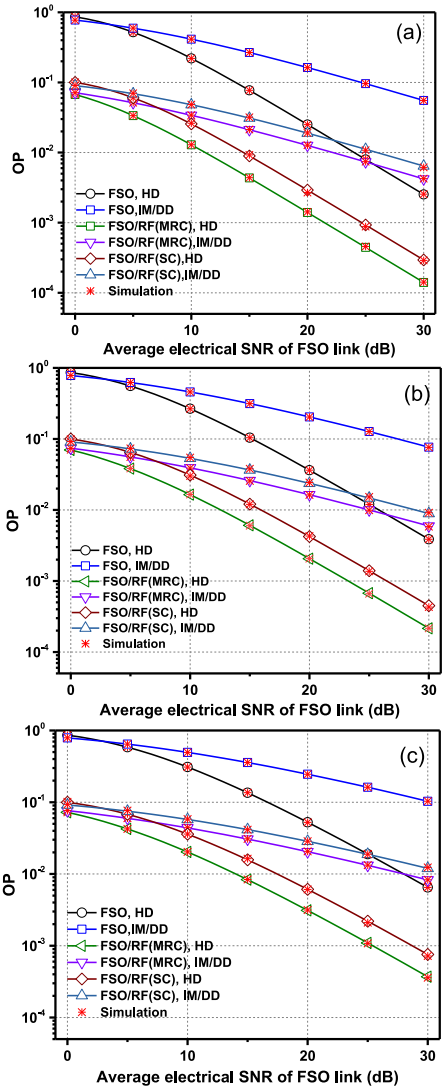

Fig. 3. OP of the single FSO link and the hybrid FSO/RF link versus average electrical SNR of the FSO link under HD and IM/DD with (a) weak, (b) moderate, (c) strong turbulent FSO channels.

$$P_e^{MRC}(\gamma) = \frac{\delta\xi^2\gamma_0^{-1-rx+tx}r^{-1}}{2\Gamma(p)\Gamma(\alpha)\Gamma(\beta)\Gamma(1+rx-tx)} \cdot q_k^{-rx+tx-1} H_{1,1;2,3;1,1}^{0,1;3,1;1,1} \sum_{k=1}^{n} \left[\begin{matrix} \alpha\beta h(\mu_r q_k)^{-1/r} \\ (q_k\gamma_0)^{-1} \end{matrix} \middle| \begin{matrix} (-p-rx+tx,1/r,1);(1,1/\rho)(\xi^2+1,1);(tx-rx,1) \\ (-1-rx+tx,1/r,1);(\xi^2,1)(\alpha,1)(\beta,1);(0,1) \end{matrix} \right] \tag{35}$$

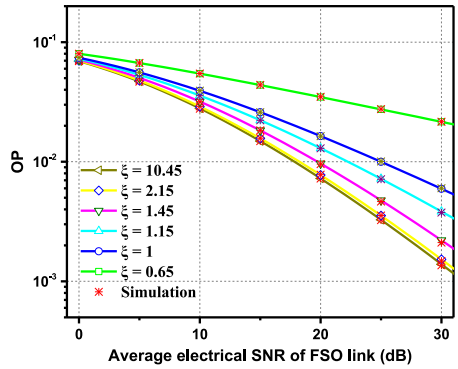

Fig. 4. OP of the hybrid FSO/RF link with varying effects of pointing errors.

The single FSO link and the hybrid FSO/RF link under moderate and strong atmospheric turbulence shown in Figs. 3(b) and Figs. 3(c) also reveal similar information as Fig. 3(a). From Fig. 3 we can also observe that the OP deteriorates along with the degradation of atmospheric turbulence. For example, when the average SNR of the FSO link is 20 dB, the OPs under weak, moderate and strong atmospheric turbulence are 2.51×10^{-2}, 3.63×10^{-2} and 5.26×10^{-2} for the single FSO link under HD and 2.91×10^{-3}, 4.30×10^{-3}, and 6.09×10^{-3} for the hybrid FSO/RF link with the SC receiver under HD, which illustrates the OP increases along with the degradation of the FSO channel.

It is worth noting that the results mentioned above are all under the pointing error $\xi = 1$, and the performance of the proposed hybrids FSO/RF link is also affected by pointing errors. Fig. 4 shows the OP of the hybrid FSO/RF system under moderate atmospheric turbulence with 5-dB average SNR of the RF link with different pointing errors ($\xi = 10.45$, 2.15, 1.45, 1.15, 1, 0.65). We can see a larger pointing error (smaller value of ξ) leads to worse system performance. Moreover, for a large variation in pointing errors from $\xi = 10.45$ to $\xi = 2.15$, there is no significant degradation in the OP performance. For instance, if OP $= 1 \times 10^{-3}$, there is a SNR loss of about 1 dB at $\xi = 2.15$ than that at $\xi = 10.45$.

As can be seen from Figs. 3 and 4, the simulated results agree well with the analytical results. This observation justifies the correctness of the derived formulas.

Under the same RF link condition, the BERs for OOK, BPSK, QPSK, and 16-QAM of the single FSO link and the FSO/RF link are also investigated using the unified BER expressions, i.e. Eqs. (8), (16) and (20). The IM/DD is employed for OOK modulation while the HD is employed for BPSK, QPSK and 16-QAM modulation. Fig. 5 shows the average BERs for different modulation schemes of the FSO link and the hybrid FSO/RF link versus the average SNR of the FSO link under the pointing error $\xi = 1$. In each sub-figure of Fig. 5, the SNR of the RF link is set to 15 dB, and the BERs of the FSO system and the FSO/RF system under weak and strong atmospheric turbulence are plotted. A good matching between the simulated and analytical BER is evident from Fig. 5.

As can be seen from Fig. 5, the BER performance is greatly improved if an extra RF link is added to the FSO link and diversity combining is utilized. In our numerical investigation,

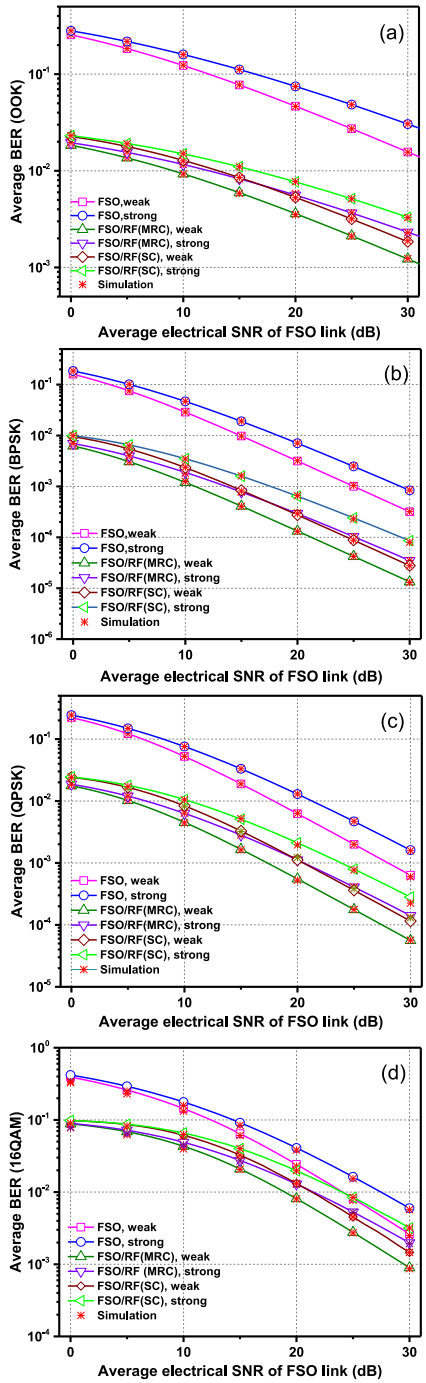

Fig. 5. Average BER for (a) OOK, (b) BPSK (c) QPSK, (d) 16QAM of the single FSO link and the hybrid FSO/RF link versus average electrical SNR of the FSO link with different average SNR of the RF link under weak and strong turbulence.

when the average SNR of the FSO link is 20 dB, the BERs for OOK, BPSK, QPSK and 16-QAM of the FSO link under strong atmospheric turbulence are 7.48×10^{-2}, 7.05×10^{-3}, 1.29×10^{-2}, and 4.09×10^{-2} while the average BERs for the hybrid FSO/RF link with the MRC receiver are reduced to 5.60×10^{-3}, 2.92×10^{-4}, 1.12×10^{-3} and 1.29×10^{-2}, respectively.

From Fig. 5, we can also observe the BER of the MRC receiver is better than that of the SC receiver. For example, when the

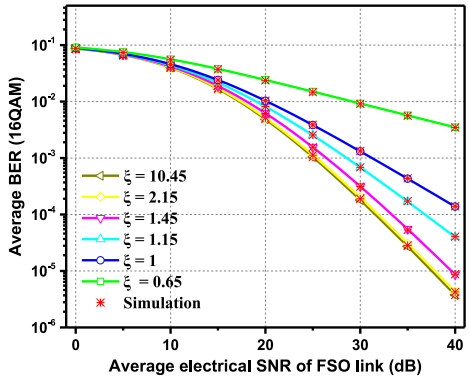

Fig. 6. Average BER for 16-QAM of the hybrid FSO/RF link with varying effects of pointing errors.

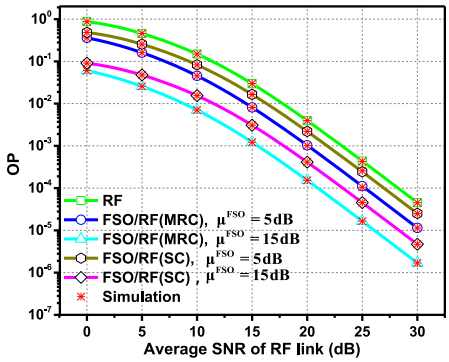

Fig. 7. OP of the single RF link and the hybrid FSO/RF link versus average SNR of the RF link with different average SNR of the FSO link.

average SNR of the FSO link is 30 dB and the turbulence is weak, the BERs of the hybrid FSO/RF system with the SC receiver for OOK, BPSK, QPSK and 16-QAM are 1.85×10^{-3}, 2.78×10^{-5}, 1.15×10^{-4}, and 1.46×10^{-3} while those with the MRC receiver are improved to 1.24×10^{-3}, 1.30×10^{-5}, 5.65×10^{-5}, and 8.95×10^{-4}, respectively.

Furthermore, we can see that as the effect of atmospheric turbulence decreases, the BER gets better. In Figs. 5(a)-(d), the BERs for OOK, BPSK, QPSK and 16-QAM of the hybrid FSO/RF system with the SC receiver are reduced from 7.73×10^{-3}, 2.40×10^{-4}, 2.11×10^{-3}, 1.97×10^{-2} to 5.31×10^{-3}, 8.76×10^{-5}, 1.12×10^{-3}, 1.32×10^{-2}, respectively, when the atmospheric turbulence turns from strong to weak.

The pointing error on the BER performance of the hybrid FSO/RF link is also investigated. Fig. 6 shows the BER for 16-QAM of the hybrid FSO/RF link with 5-dB average SNR of the RF link under moderate atmospheric turbulence with different ξ parameters ($\xi = 10.45, 2.15, 1.45, 1.15, 1, 0.65$). Similar to the OP, a larger pointing error also leads to worse BER performance. Moreover, when the ξ characterizing the pointing error changes from a large value ($\xi = 10.45$) to a small value ($\xi = 2.15$) in our investigation, the BER performance does not degrade significantly. For example, at BER $= 1 \times 10^{-3}$, there is a SNR loss less than 0.5 dB at $\xi = 2.15$ than that at $\xi = 10.45$.

For the single RF link, the performance can also be improved if an extra FSO link is added and diversity combining is implemented. A more general RF fading channel which is κ-μ shadowed fading ($\kappa = 10$, $\mu = 2$ and $m = 1$) is considered in this case. For the FSO link, the atmospheric turbulence is set to moderate ($\alpha = 2.296$, $\beta = 1.822$), and the pointing error parameter ξ is set to 1.

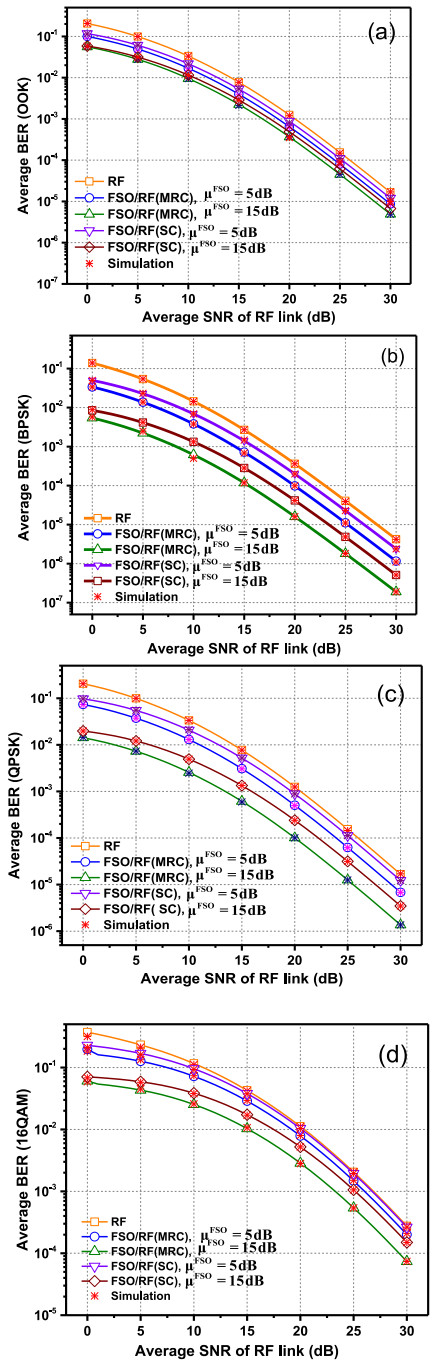

Fig. 8. Average BER for (a) OOK (b) BPSK (c) QPSK (d) 16-QAM of the single RF link and the hybrid FSO/RF link versus average SNR of the RF link with different average SNR of the FSO link.

Fig. 7 shows the OP versus average SNR of the single RF link and the hybrid FSO/RF link with 5-dB and 15-dB average SNRs of the FSO link, respectively. We can see from Fig. 7 that the OP performance is improved if an extra FSO link is added to the RF link. For instance, when the average SNR of the RF link is

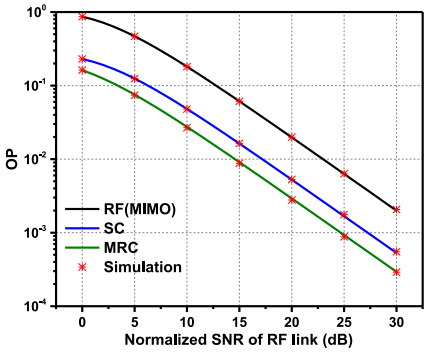

Fig. 9. OP of the MIMO RF link and the hybrid FSO/RF link versus average SNR of the RF link.

20 dB, the OP is 3.96×10^{-3} while for the hybrid FSO/RF link under HD, the OP performance of the hybrid FSO/RF link with the MRC receiver is improved to 1.03×10^{-3} and 1.53×10^{-4} when the average SNRs of the FSO links are 5 dB and 15 dB, respectively.

Moreover, using the unified BER expressions given in Eq. (13), (16) and (20), the average BERs for different modulation schemes are presented. Figs. 8(a)–(d) show the BERs for OOK, BPSK, QPSK and 16-QAM of the single RF link and the hybrid FSO/RF link. In all cases, the average BER is reduced if an extra FSO link is enabled. According to our numerical investigation, the BERs for OOK, BPSK, QPSK, and 16-QAM of the single RF link are 1.25×10^{-3}, 3.63×10^{-4}, 1.25×10^{-3} and 1.12×10^{-2} of the single RF link while those of the hybrid FSO/RF link with the MRC receiver are reduced to 3.66×10^{-4}, 1.61×10^{-5}, 1.01×10^{-4} and 2.86×10^{-3}, respectively, when the average SNR of the FSO link is 15 dB.

If a better FSO link is enabled, the performance of the hybrid FSO/RF link will be further improved. For example, when the average SNR of the single RF link is 20 dB, the BER for OOK is 1.25×10^{-3}. If the FSO link with 5-dB average SNR is enabled and the MRC receiver is used, the BER is improved to 6.46×10^{-4}. If the average SNR of the FSO link increases to 15 dB, the BER is further improved to 3.66×10^{-4}.

It can be observed from Figs. 7 and 8 that the simulation results match exactly to the derived analytical expressions obtained in this work.

B. Hybrid FSO and MIMO RF Link

The performance of the hybrid FSO and MIMO RF link is also numerically investigated. In the simulation, the moderate turbulence is assumed, and the average electrical SNR of the FSO link is 10 dB.

The OPs of the MIMO RF link and the hybrid link with SC and MRC receivers are given in Fig. 9. We can see from Fig. 9 that the hybrid link has better OP performance than the MIMO RF link. For instance, when the normalized received SNR of the RF link is 20 dB, the OP is 1.98×10^{-2} while for the hybrid FSO/RF link under IM/DD, the OP performance of the hybrid FSO/RF link is improved to 5.30×10^{-3} by the SC receiver and 2.78×10^{-3} by the MRC receiver.

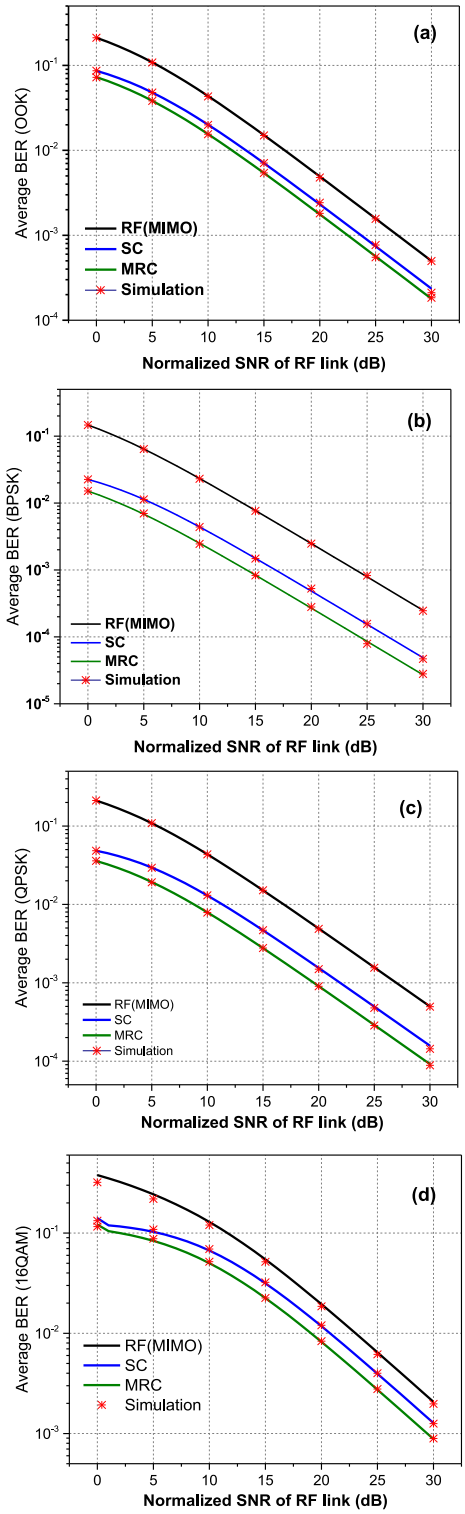

Fig. 10. Average BER for (a) OOK (b) BPSK (c) QPSK (d) 16-QAM of the MIMO RF link and the hybrid FSO/RF link versus average SNR of the RF link.

The BER performance of the hybrid link is also presented. The BER of OOK, BPSK, QPSK and 16QAM of the MIMO RF link and the hybrid RF/FSO link is shown in Figs. 10(a–d), respectively. We can conclude from Fig. that the BER can be reduced if an FSO link is combined with RF link,

and the MRC has better performance than SC. For example, when the normalized RF SNR is 20 dB, the BER of OOK of the MIMO RF link is 4.93×10^{-3} while the hybrid link with SC and MRC is 2.42×10^{-3} and 1.81×10^{-3}, respectively.

IV. Conclusion

In summary, we analyzed the performance of hybrid FSO/RF systems with diversity combining which can be integrated in fiber-wireless MBH. We offered exact closed-form expressions of the OP and average BERs for different modulation schemes in terms of the Fox's H function. Since unified models of FSO and RF links are utilized, respectively, the derived expressions are very general, which accounts for atmospheric turbulence, pointing errors and two types of detection techniques (i.e. HD and IM/DD) for the FSO link and different RF fading models for the RF link. A preliminary extension of the RF link to multi-input multi-output (MIMO) transmission is also analyzed. Numerical results show the hybrid FSO/RF system with MRC has superior outage performance compared to single FSO systems and single RF systems in all atmospheric turbulence regimes, pointing errors and RF fading. The derived formulas verified by Monte-Carlo simulations, which are given in Sections II and III, can help to evaluate different hybrid FSO/RF scenarios.

Appendix

A. Derivation of Average BER of FSO Link

In this appendix, we derive the average BER of the single FSO link that accounts for the HD and IM/DD as well as point errors. By substituting Eq. (6) to Eq. (7), the average BER of the single FSO link can be given by

$$\begin{aligned} P_e^{FSO} &= \frac{\delta}{2\Gamma(p)} \sum_{k=1}^{n} q_k^p \int_0^\infty {\gamma_r}^{p-1} e^{-q_k \gamma_r} F_\gamma^{FSO}(\gamma_r) d\gamma_r \\ &= \frac{\delta}{2\Gamma(p)} \sum_{k=1}^{n} q_k^p \int_0^\infty {\gamma_r}^{p-1} e^{-q_k \gamma_r} \\ &\quad \times \left\{ 1 - \frac{\xi^2}{\Gamma(\alpha)\Gamma(\beta)} G_{2,4}^{4,0}\left[\alpha\beta h (\frac{\gamma_r}{\mu_r})^{\frac{1}{r}} \,\middle|\, \begin{matrix} 1, \xi^2+1 \\ 0, \xi^2, \alpha, \beta \end{matrix} \right] \right\} d\gamma_r \\ &= \frac{\delta}{2\Gamma(p)} \sum_{k=1}^{n} q_k^p \left(I_1 - I_2 \right) \end{aligned} \tag{36}$$

where

$$I_1 = \int_0^\infty {\gamma_r}^{p-1} e^{-q_k \gamma} d\gamma_r = q_k^{-p} \Gamma(p) \tag{37}$$

by using [22, Eq. (3.381.4)], and

$$\begin{aligned} I_2 &= \int_0^\infty {\gamma_r}^{p-1} e^{-q_k \gamma_r} \frac{\xi^2}{\Gamma(\alpha)\Gamma(\beta)} G_{2,4}^{4,0}\left[\alpha\beta h \left(\frac{\gamma_r}{\mu_r} \right)^{\frac{1}{r}} \,\middle|\, \begin{matrix} 1, \xi^2+1 \\ 0, \xi^2, \alpha, \beta \end{matrix} \right] d\gamma_r \\ &= \frac{\xi^2}{\Gamma(\alpha)\Gamma(\beta)} \cdot \int_0^\infty {\gamma_r}^{p-1} e^{-q_k \gamma_r} \\ &\quad \cdot \frac{1}{2\pi j} \int_L \frac{\Gamma(-s)\Gamma(\xi^2 - s)\Gamma(\alpha - s)\Gamma(\beta - s)}{\Gamma(1-s)\Gamma(\xi^2 + 1 - s)} \\ &\quad \times \left[\alpha\beta h (\frac{\gamma_r}{\mu_r})^{\frac{1}{r}} \right]^s ds \cdot d\gamma_r \\ &= \frac{\xi^2}{\Gamma(\alpha)\Gamma(\beta)} \cdot \frac{1}{2\pi j} \int_L \frac{\Gamma(-s)\Gamma(\xi^2 - s)\Gamma(\alpha - s)\Gamma(\beta - s)}{\Gamma(1-s)\Gamma(\xi^2 + 1 - s)} \\ &\quad \times \left[\alpha\beta h \left(\frac{1}{\mu_r} \right)^{\frac{1}{r}} \right]^s ds \int_0^\infty {\gamma_r}^{p-1+s/r} e^{-q_k \gamma_r} d\gamma_r \\ &= \frac{\xi^2}{\Gamma(\alpha)\Gamma(\beta)} \cdot \frac{1}{2\pi j} \int_L q_k^{-p-s/r} \Gamma(p + s/r) \\ &\quad \times \frac{\Gamma(-s)\Gamma(\xi^2 - s)\Gamma(\alpha - s)\Gamma(\beta - s)}{\Gamma(1-s)\Gamma(\xi^2 + 1 - s)} \left[\alpha\beta h \left(\frac{1}{\mu_r} \right)^{\frac{1}{r}} \right]^s ds \\ &= \frac{\xi^2}{\Gamma(\alpha)\Gamma(\beta)} \\ &\quad \cdot q_k^{-p} H_{3,4}^{4,1}\left[\alpha\beta h (q_k \mu_r)^{-\frac{1}{r}} \,\middle|\, \begin{matrix} (1-p, 1/r)(1,1)(\xi^2+1, 1) \\ (0,1)(\xi^2, 1)(\alpha, 1)(\beta, 1) \end{matrix} \right], \end{aligned} \tag{38}$$

by using [22, Eq. (3.381.4)] and [24].

Finally, by substituting Eqs. (22) and (23) to Eq. (21), Eq. (21) can be written as Eq. (8).

B. Derivation of Average BER of FSO/RF Link With SC Receiver

Substituting Eq. (15) to Eq. (7), the average BER of the hybrid FSO/RF link with the SC receiver can be expressed as Eq. (39) shown at the bottom of the next page, where

$$\begin{aligned} P_1 = \frac{n\delta}{2} - \frac{\delta \xi^2}{2\Gamma(p)\Gamma(\alpha)\Gamma(\beta)} \sum_{k=1}^{n} H_{3,4}^{4,1} \\ \left[\alpha\beta h (q_k \mu_r)^{-\frac{1}{r}} \,\middle|\, \begin{matrix} (1-p, 1/r)(1,1)(\xi^2+1, 1) \\ (0,1)(\xi^2, 1)(\alpha, 1)(\beta, 1) \end{matrix} \right], \end{aligned} \tag{40}$$

by using [22, Eq. (3.381.4)] and [24],

$$P_2 = \frac{\delta}{2\Gamma(p)} \sum_{k=1}^{n} \sum_{i=0}^{M} \sum_{r=0}^{m_i - 1} \frac{C_i \Gamma(p+r)}{r!} \frac{1}{\Omega_i^r (q_k + \Omega_i^{-1})^{p+r}}, \tag{41}$$

by using [22, Eq. (3.381.4)], and

$$\begin{aligned} P_3 = \frac{\delta}{2\Gamma(p)} \frac{\xi^2}{\Gamma(\alpha)\Gamma(\beta)} \sum_{k=1}^{n} \sum_{i=0}^{M} \sum_{\rho=0}^{m_i - 1} \frac{q_k^p C_i}{r! \Omega_i^r \left(q_k + \Omega_i^{-1} \right)^{p+r}} H_{3,4}^{4,1} \\ \left[\alpha\beta h \left((q_k + \Omega_i^{-1}) \mu_r \right)^{-1/r} \,\middle|\, \begin{matrix} (1-p-r, 1/r)(1,1)(\xi^2+1, 1) \\ (0,1)(\xi^2, 1)(\alpha, 1)(\beta, 1) \end{matrix} \right], \end{aligned} \tag{42}$$

by using [22, Eq. (3.381.4)] and [24].

Finally, by substituting Eqs. (25)-(27) to Eq. (24), Eq. (24) can be written as Eq. (16).

C. Derivation of CDF of Hybrid FSO/RF System With MRC Receiver

We apply inverse Laplace transform to, and use [22, Eq. (9.301)] and [28, Eq.(1.1)]. Then the CDF of the hybrid FSO/RF link can be written as

$$\begin{aligned}
&F_{\gamma}^{MRC}(\gamma)\\
&=\frac{1}{2\pi j}\int_{\sigma-j\infty}^{\sigma+j\infty}\frac{M_{\gamma}^{MRC}(-s)}{s}e^{s\gamma}ds\\
&=\frac{1}{2\pi j}\frac{\xi^2}{r\Gamma(\alpha)\Gamma(\beta)}\sum_{i=0}^{M}\frac{C_i}{(m_i-1)!}\\
&\quad\cdot\int_{\sigma+j\infty}^{\sigma+j\infty}G_{1,1}^{1,1}\left[s\Omega_i\left|{}_{0}^{1-m_i}\right.\right]H_{2,3}^{3,1}\\
&\quad\left[\alpha\beta h(\mu_r s)^{-1/r}\left|\begin{matrix}(1,1/r)(\xi^2+1,1)\\(\xi^2,1)(\alpha,1)(\beta,1)\end{matrix}\right.\right]s^{-1}e^{s\gamma}ds\\
&=\frac{\xi^2}{r\Gamma(\alpha)\Gamma(\beta)}\sum_{i=0}^{M}\frac{C_i}{(m_i-1)!}\cdot\left(\frac{1}{2\pi j}\right)^2\\
&\quad\cdot\int_{L_1}\int_{L_2}\Gamma(-u)\Gamma(m_i+u)\Omega_i^u\\
&\quad\times\frac{\Gamma(\xi^2+t)\Gamma(\alpha+t)\Gamma(\beta+t)\Gamma(-t/r)}{\Gamma(\xi^2+1+t)}\left(\frac{\mu_r^{\frac{1}{r}}}{\alpha\beta h}\right)^t dudt\\
&\quad\cdot\left(\frac{1}{2\pi j}\right)\int_{\sigma-j\infty}^{\sigma+j\infty}s^{u+t/r-1}e^{sr}ds. \qquad (43)
\end{aligned}$$

Using [22, Eq.(17.13.1)], Eq. (28) can be further written as (44) shown at the bottom of this page, where $H[.,.]$ is the bivariate Fox's H function which is defined in [28, A.1].

D. Derivation of Average BER of Hybrid FSO/RF System With MRC Receiver

We substitute Eq. (19) to Eq. (7) and utilize [29, Eq. (1.11)], and then the average BER of the hybrid FSO/RF systems can be given by

$$\begin{aligned}
&P_e^{MRC}\\
&=\frac{\delta}{2\Gamma(p)}\sum_{k=1}^{n}q_k^p\int_0^{\infty}\gamma^{p-1}e^{-q_k\gamma}F_{\gamma}^{MRC}(\gamma)d\gamma\\
&=\frac{\delta}{2\Gamma(p)}\sum_{k=1}^{n}q_k^p\int_0^{\infty}\gamma^{p-1}e^{-q_k\gamma}
\end{aligned}$$

$$\begin{aligned}
P_e^{SC}&=\frac{\delta}{2\Gamma(p)}\sum_{k=1}^{n}q_k^p\int_0^{\infty}\gamma^{p-1}e^{-q_k\gamma}F_{\gamma}^{SC}(\gamma)d\gamma\\
&=\underbrace{\frac{\delta}{2\Gamma(p)}\sum_{k=1}^{n}q_k^p\int_0^{\infty}d\gamma\cdot\gamma^{p-1}e^{-q_k\gamma}\left\{1-\frac{\xi^2}{\Gamma(\alpha)\Gamma(\beta)}G_{2,4}^{4,0}\left[\alpha\beta h\left(\frac{\gamma_r}{\mu_r}\right)^{\frac{1}{r}}\left|\begin{matrix}1,\xi^2+1\\0,\xi^2,\alpha,\beta\end{matrix}\right.\right]\right\}}_{P_1}\\
&\quad-\underbrace{\frac{\delta}{2\Gamma(p)}\sum_{k=1}^{n}q_k^p\int_0^{\infty}d\gamma\cdot\gamma^{p-1}e^{-q_k\gamma}\left[\sum_{i=0}^{M}\sum_{r=0}^{m_i-1}\frac{C_i}{r!}e^{-\frac{\gamma}{\Omega_i}}\left(\frac{\gamma}{\Omega_i}\right)^r\right]}_{P_2}\\
&\quad+\underbrace{\frac{\delta}{2\Gamma(p)}\sum_{k=1}^{n}q_k^p\int_0^{\infty}d\gamma\cdot\gamma^{p-1}e^{-q_k\gamma}\left\{\frac{\xi^2}{\Gamma(\alpha)\Gamma(\beta)}\sum_{i=0}^{M}\sum_{r=0}^{m_i-1}\frac{C_i}{r!}e^{-\frac{\gamma}{\Omega_i}}\left(\frac{\gamma}{\Omega_i}\right)^r G_{2,4}^{4,0}\left[\alpha\beta h\left(\frac{\gamma}{\mu_r}\right)^{\frac{1}{r}}\left|\begin{matrix}1,\xi^2+1\\0,\xi^2,\alpha,\beta\end{matrix}\right.\right]\right\}}_{P_3}, \qquad (39)
\end{aligned}$$

$$\begin{aligned}
F_{\gamma}^{MRC}(\gamma)&=\frac{\xi^2}{r\Gamma(\alpha)\Gamma(\beta)}\sum_{i=0}^{M}\frac{C_i}{(m_i-1)!}\cdot(\frac{1}{2\pi j})^2\\
&\quad\int_{L_1}\int_{L_2}\frac{\Gamma(-u)\Gamma(m_i+u)\Gamma(\xi^2+t)\Gamma(\alpha+t)\Gamma(\beta+t)\Gamma(-t/r)}{\Gamma(\xi^2+1+t)\Gamma(-u-t/r+1)}\left(\frac{\Omega_i}{\gamma}\right)^u\left(\frac{\left(\frac{\mu_r}{\gamma}\right)^{\frac{1}{r}}}{\alpha\beta h}\right)^t dudt\\
&=\frac{\xi^2}{r\Gamma(\alpha)\Gamma(\beta)}\\
&\quad\sum_{i=0}^{M}\frac{C_i}{(m_i-1)!}H_{1,0:1,1:3,2}^{0,0:1,1:1,3}\left[\begin{matrix}\Omega_i/\gamma\\\left(\frac{\mu_r}{\gamma}\right)^{\frac{1}{r}}/(\alpha\beta h)\end{matrix}\left|\begin{matrix}(-)(1,1,1/r):(1-m_i,1):(1-\xi^2,1)(1-\alpha,1)(1-\beta,1)\\(-):(0,1):(0,1/r)(-\xi^2,1)\end{matrix}\right.\right] \qquad (44)
\end{aligned}$$

$$P_e^{MRC} = \frac{\delta\xi^2}{2r\Gamma(p)\Gamma(\alpha)\Gamma(\beta)} \sum_{k=1}^{n}\sum_{i=0}^{M} \frac{C_i}{(m_i-1)!}\left(\frac{1}{2\pi j}\right)^2 \int_{L_1}\int_{L_2} \frac{\Gamma(u)\Gamma(m_i-u)\Gamma(\xi^2-t)\Gamma(\alpha-t)\Gamma(\beta-t)\Gamma(t/r)\Gamma(p+u+t/r)}{\Gamma(\xi^2+1-t)\Gamma(u+t/r+1)\Gamma(1+u+t/r)} (q_k\Omega_i)^u \left[\alpha\beta h(\mu_r q_k)^{-1/r}\right]^t dudt$$
$$= \frac{\delta\xi^2}{2r\Gamma(p)\Gamma(\alpha)\Gamma(\beta)} \sum_{k=1}^{n}\sum_{i=0}^{M} \frac{C_i}{(m_i-1)!} H_{1,1:1,1:2,3}^{0,1:1,1:3,1}\left[\begin{matrix}(q_k\Omega_i)^{-1}\\ \alpha\beta h(\mu_r q_k)^{-1/r}\end{matrix}\middle|\begin{matrix}(p,1,1/r):(1,1):(1,1/r)(\xi^2+1,1)\\ (0,1,1/r):(m_i,1):(\xi^2,1)(\alpha,1)(\beta,1)\end{matrix}\right] \quad (46)$$

$$\cdot\left[\frac{\xi^2}{r\Gamma(\alpha)\Gamma(\beta)}\sum_{i=0}^{M}\frac{C_i}{(m_i-1)!}\left(\frac{1}{2\pi j}\right)^2 \cdot\int_{L_1}\int_{L_2}\frac{\Gamma(u)\Gamma(m_i-u)\Gamma(\xi^2-t)\Gamma(\alpha-t)\Gamma(\beta-t)\Gamma(t/r)}{\Gamma(\xi^2+1-t)\Gamma(u+t/r+1)} \times\left(\frac{\gamma}{\Omega_i}\right)^u\left(\alpha\beta h\left(\frac{\gamma}{\mu_r}\right)^{\frac{1}{r}}\right)^t dudt\right]d\gamma$$
$$= \frac{\delta\xi^2}{2r\Gamma(p)\Gamma(\alpha)\Gamma(\beta)}\sum_{k=1}^{n}\sum_{i=0}^{M}\frac{q_k^p C_i}{(m_i-1)!}\left(\frac{1}{2\pi j}\right)^2 \cdot\int_{L_1}\int_{L_2}\frac{\Gamma(u)\Gamma(m_i-u)\Gamma(\xi^2-t)\Gamma(\alpha-t)\Gamma(\beta-t)\Gamma(t/r)}{\Gamma(\xi^2+1-t)\Gamma(u+t/r+1)} \times\left(\frac{1}{\Omega_i}\right)^u\left(\alpha\beta h\left(\frac{1}{\mu_r}\right)^{\frac{1}{r}}\right)^t dudt\int_0^\infty \gamma^{p-1+u+t/r}e^{-q_k\gamma}d\gamma. \quad (45)$$

By using [22, Eq. (3.381.4)], Eq. (30) can be finally written as Eq. (46) shown at the top of this page.

REFERENCES

[1] S. Bloom and W. Hartley, "The last-mile solution: Hybrid FSO radio," white paper, AirFiber Inc., 802-0008-000 M-A1, pp. 1–20, May 2002.

[2] A. Al-Habash, L. Andrews, and R. Phillips, "Mathematical model for the irradiance probability density function of a laser beam propagating through turbulent media," *Opt. Eng.*, vol. 40, no. 8, pp. 1554–1562, 2001.

[3] W. Gappmair, "Further results on the capacity of free-space optical channels in turbulent atmosphere," *IET Commun.*, vol. 5, no. 9, pp. 1262–1267, Aug. 2011.

[4] J. Park, E. Lee, and G. Yoon, "Average bit-error rate of the Alamouti scheme in Gamma-Gamma fading channels," *IEEE Photon. Technol. Lett.*, vol. 23, no. 4, pp. 269–271, Feb. 2011.

[5] M. Niu, J. Cheng, and J. F. Holzman, "Exact error rate analysis of equal gain and selection diversity for coherent free-space optical systems on strong turbulence channels," *Opt. Express*, vol. 18, no. 13, pp. 13915–13926, Jun. 2010.

[6] F. Nadeem, V. Kvicera, M. Awan, E. Leitgeb, S. Muhammad, and G. Kandus, "Weather effects on hybrid FSO/RF communication link," *IEEE J. Sel. Areas Commun.*, vol. 27, no. 9, pp. 1687–1697, Dec. 2009.

[7] A. AbdulHussein, A. Oka, T. T. Nguyen, and L. Lampe, "Rateless coding for hybrid free-space optical and radio-frequency communication," *IEEE Trans. Wireless Commun.*, vol. 9, no. 3, pp. 907–913, Mar. 2010.

[8] B. He and Robert Schober, "Bit-interleaved coded modulation for hybrid RF/FSO systems," *IEEE Trans. Commun.*, vol. 57, no. 12, pp. 3753–3763, Dec. 2009.

[9] W. Zhang, S. Hranilovic, and C. Shi, "Soft-switching hybrid FSO/RF links using short-length raptor codes: Design and implementation," *IEEE J. Sel. Areas Commun.*, vol. 27, no. 9, pp. 1698–1708, Dec. 2009.

[10] J. Zhang *et al.*, "Fiber–wireless integrated mobile backhaul network based on a hybrid millimeter-wave and free-space-optics architecture with an adaptive diversity combining technique," *Opt. Lett.*, vol. 41, no. 9, pp. 1909–1912, May 2016.

[11] J. Yu, X. Li, and N. Chi, "Faster than fiber: over 100-Gb/s signal delivery in fiber wireless integration system," *Opt. Express*, vol. 21, no. 19, pp. 22885–22904, 2013.

[12] L. Huang *et al.*, "Simple multi-RAT RoF system with 2X2 MIMO wireless transmission," *IEEE Photon. Technol. Lett.* vol. 31, no. 13, pp. 1025–1028, May 2019.

[13] X. Li *et al.*, "120 Gb/s wireless terahertz-wave signal delivery by 375 GHz–500 GHz multi-carrier in a 2 × 2 MIMO system," *IEEE J. Lightw. Technol.*, vol. 37, no. 2, pp. 606–611, Jan. 2019.

[14] A. Kanno *et al.*, "40 Gb/s W-band (75–110 GHz) 16-QAM radio-over-fiber signal generation and its wireless transmission," *Opt. Express*, vol. 19, no. 26, pp. 56–63, 2011.

[15] M. Usman, H.-C. Yang, and M.-S. Alouini, "Practical switching-based hybrid FSO/RF transmission and its performance analysis," *IEEE Photon. J.*, vol. 6, no. 5, pp. 1–13, Oct. 2014.

[16] N. D. Chatzidiamantis, G. K. Karagiannidis, E. E. Kriezis, and M. Matthaiou, "Diversity combining in hybrid RF/FSO systems with PSK modulation," in *Proc. IEEE Int. Conf. Commun.*, Kyoto, Japan, Jun. 2011, pp. 1–6.

[17] T. Rakia, H.-C. Yang, M.-S. Alouini, and F. Gebali, "Outage analysis of practical FSO/RF hybrid system with adaptive combining," *IEEE Commun. Lett.*, vol. 19, no. 8, pp. 1366–1369, Aug. 2015.

[18] W. M. R. Shakir, "Performance evaluation of a selection combining scheme for the hybrid FSO/RF system," *IEEE Photon. J.*, vol. 10, no. 1, pp. 1–10, Feb. 2018.

[19] M. A. Amirabadi and V. T. Vakili, "Performance evaluation of a novel relay-assisted hybrid FSO/RF communication system with receive diversity," *IET Optoelectron.*, vol. 13, no. 5, pp. 203–214, 2019.

[20] J. F. Paris, "Statistical characterization of κ;-μ; shadowed fading," *IEEE Trans. Veh. Technol.*, vol. 63, no. 2, pp. 518–526, Feb. 2014.

[21] F. J. Lopez-Martinez, J. F. Paris, and J. M. Romero-Jerez, "The κ;-μ; shadowed fading model with integer fading parameters," *IEEE Trans. Veh. Technol.*, vol. 66, no. 9, pp. 7653–7662, Sep. 2017.

[22] I. S. Gradshteyn and I. M. Ryzhik, *Table of Integrals, Series, and Products*. New York, NY, USA: Academic, 2000.

[23] E. Zedni, H. Soury, and M.-S. Alouini, "Dual-hop FSO transmission systems over Gamma-Gamma turbulence with pointing errors," *IEEE Trans. Wireless Commun.*, vol. 16, no. 2, pp. 784–796, Feb. 2017.

[24] E. W. Weisstein, "Fox H-Function – from Wolfram MathWorld, Mathworld.wolfram.com, 2020. [Online]. Available: https://mathworld.wolfram.com/FoxH-Function.html. Accessed: Sep. 17, 2020.

[25] L. Huang *et al.*, "Simple multi-RAT RoF system with 2 × 2 MIMO wireless transmission," *IEEE Photon. Technol. Lett.*, vol. 31, no. 13, pp. 1025–1028, Jul. 2019.

[26] C.-T. Lin *et al.*, "2 × 2 MIMO radio-over-fiber system at 60 GHz employing frequency domain equalization," *Opt. Express*, vol. 20, no. 1, pp. 562–567, 2012.

[27] R. Xu and F. C. M. Lau, "Performance analysis for MIMO systems using zero forcing detector over fading channels," *IEE Proc. Commun.*, vol. 153, pp. 74–80, Feb. 2006.

[28] A. M. Mathai, R. K. Saxena, and H. J. Haubold, *The H-Function: Theory and Applications*. New York, NY, USA: Springer, 2010.

[29] N. T. Hai and S B Yakubovich, *The Double Mellin-Barnes Type Integrals and Their Applications to Convolution Theory*. Singapore: World Scientific, 1992.

[30] X. Tang, Z. Ghassemlooy, S. Rajbhandari, W. O. Popoola, and C. G. Lee, "Coherent polarization shift keying modulated free space optical links over a Gamma-Gamma turbulence channel," *Amer. J. Eng. Appl. Sci.*, vol. 4, no. 4, pp. 520–530, 2011.